Near Rectilinear Halo Orbit Determination with Simulated DSN Observations

Nathan L. Parrish[1], Matthew J. Bolliger[2], Ethan Kayser[3],
Michael R. Thompson[4], Jeffrey S. Parker[5], Bradley W. Cheetham[6]
Advanced Space LLC, 2100 Central Ave, Boulder, CO 80301

Diane C. Davis[7]
ai solutions, 2224 Bay Area Blvd #415, Houston, TX 77058

Daniel J. Sweeney[8]
NASA Johnson Space Center, Houston TX 77048

This paper presents the results of both a high-fidelity simulation of spacecraft orbit determination in a near rectilinear halo orbit (NRHO), as well as investigations of various aspects of NRHO operations, including NRHO insertion and long-horizon orbit maintenance. Others in the literature have examined the NRHO navigation problem with linear covariance analysis, but the highly-nonlinear dynamics of this orbit challenge the assumptions underlying such analyses. The present work builds on similar analysis performed by other authors to contribute a fuller understanding of the operational requirements for NRHO navigation. The present work serves as a check to the assumptions of previous studies and an independent verification of those results. Various trades are performed, including: NRHO insertion cleanup, short-horizon and long-horizon orbit maintenance, tracking cadence, tracking pass placement, filter type, measurement noise, and measurement type. Spacecraft state uncertainty estimates are evaluated as a function of time. Simulated range and range-rate measurements with the Deep Space Network (DSN) ground stations are used to model orbit determination accuracy. Orbit maintenance maneuvers are performed using both short-horizon and long-horizon stationkeeping targeting. Monte Carlo analysis of orbit determination and stationkeeping is performed.

I. Introduction

NASA's current plans for human and robotic exploration include a renewed focus on the Moon. Two upcoming missions, the crew-tended Gateway and the robotic CAPSTONE spacecraft, plan to exploit low-cost mission opportunities offered by multibody orbits. Both spacecraft plan to primarily reside in Near Rectilinear Halo Orbits (NRHOs) near the Moon. Nearly-stable members of the halo orbit families, southern L_2 NRHOs have low ΔV requirements for orbit maintenance, and they offer extensive coverage of the lunar south pole, fast and relatively inexpensive access to the lunar surface, and favorable aborts back to the Earth.[1] To achieve inexpensive orbit maintenance, safe rendezvous, and reliable disposal of spacecraft from NRHO, accurate orbit determination (OD) within the NRHO is required.

Many missions, including ICEE-3, Genesis, ACE, SOHO and Wind,[2] have successfully operated in Sun-Earth halo orbits. The upcoming JWST and WFIRST[3] missions are also planned to reside in Sun-Earth halos. A single

[1] Optimization Lead, Advanced Space, LLC, 2100 Central Ave STE 102, Boulder, CO 80301. AIAA member.
[2] Aerospace Engineer, Advanced Space, LLC, 2100 Central Ave STE 102, Boulder, CO 80301. AIAA member.
[3] Aerospace Engineer, Advanced Space, LLC, 2100 Central Ave STE 102, Boulder, CO 80301. AIAA member.
[4] Aerospace Engineer, Advanced Space, LLC, 2100 Central Ave STE 102, Boulder, CO 80301. AIAA member.
[5] Chief Technology Officer, Advanced Space, LLC, 2100 Central Ave STE 102, Boulder, CO 80301. AIAA member.
[6] Chief Executive Officer, Advanced Space, LLC, 2100 Central Ave STE 102, Boulder, CO 80301. AIAA member.
[7] Principal Systems Engineer, ai solutions, 2224 Bay Area Blvd #415, Houston TX 77058. AIAA member.
[8] Gateway Integrated Spacecraft Performance Lead, NASA Johnson Space Center, Houston, TX 77058. AIAA member.

mission to date, the 2010 ARTEMIS mission that served as an end-of-life opportunity for two of the THEMIS spacecraft, has demonstrated successful operations, including accurate OD, in Earth-Moon halo orbits.[4] The CAPSTONE mission, scheduled to launch in December 2020, and the Gateway starting in 2022 will be the first spacecraft to operate in NRHOs.

NRHOs represent a subset of the L_1 and L_2 halo orbits, bounded by changes in linear stability. Some NRHOs are linearly stable in the Earth-Moon circular restricted three-body dynamics; others are slightly unstable. The current nominal orbit for the Gateway is a 9:2 synodic resonant southern L_2 NRHO, meaning that the spacecraft completes 9 revolutions about the Moon for every 2 synodic revolutions of the Moon about the Earth. This resonance is favorable because it minimizes the amount of time spent in the Earth's shadow while offering favorable lunar surface access. NRHOs with a 9:2 resonance are linearly unstable. However, small maneuvers can maintain a safe orbit for a ΔV cost on the order of a few meters per second per year. A 9:2 resonant NRHO appears in the Earth-Moon rotating frame Figure 1a.

Certain characteristics of NRHOs complicate orbit determination. For example, when propagated in a high-fidelity ephemeris model, an NRHO is quasi-periodic in the Earth-Moon rotating frame, and the orbital plane is approximately perpendicular to the line-of-sight from Earth. This geometry leads to navigational challenges, since Earth-based range and range-rate measurements cannot directly measure the main orbital motion; the system is poorly observable. Additionally, NRHOs are characterized by large variations in the distance to the Moon; the radius of the 9:2 NRHO ranges from approximately 3,500 km at perilune to about 71,000 km at apolune. These significant differences cause the acceleration experienced by the spacecraft to vary by 2-3 orders of magnitude within a single revolution. The variation in acceleration experienced by a spacecraft in an NRHO is compared to the variation in acceleration experienced by a spacecraft in low lunar orbit (LLO) in Figure 1b. This extreme change in dynamics is comparable (in terms of navigational challenge) to performing a lunar flyby once every week.

Further navigational complications arise from the limited control authority available to a spacecraft with solar electric propulsion (SEP), such as the Power and Propulsion Element (PPE) of the Gateway. It is apparent in Figure 1b that the SEP control acceleration is considerably less than the gravity of the Moon and Earth at all times. If the orbit determination filter fails to track the spacecraft, there is a potential risk that the spacecraft's path could diverge beyond the point of recoverability by the SEP thrusters. That is, there is some amount of spacecraft state error beyond which the spacecraft's limited control authority is inadequate to return to the nominal NRHO without large corrections or the use of an alternative propulsion system such as RCS thrusters.

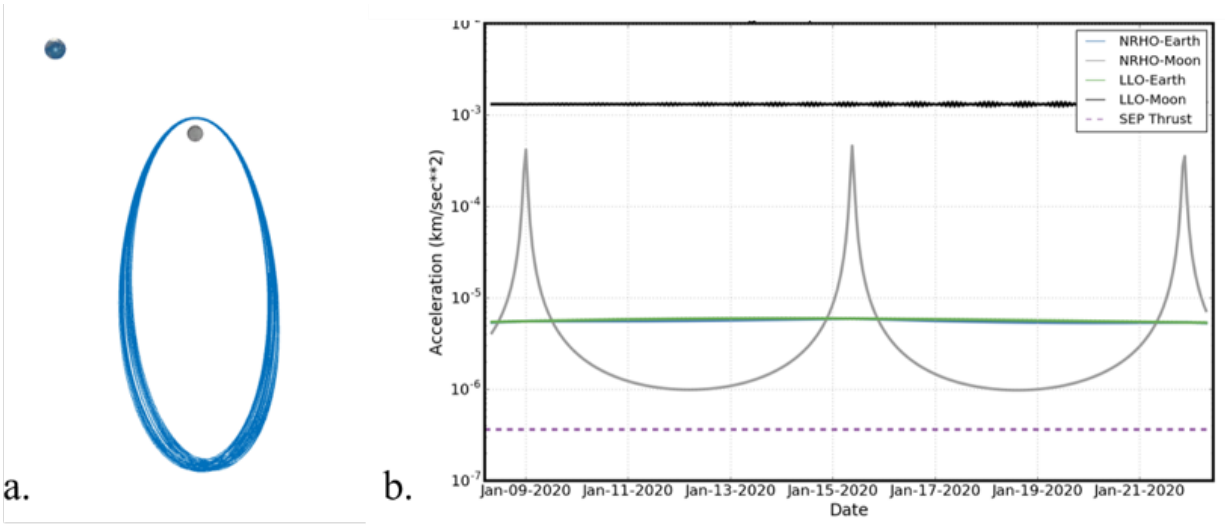

Figure 1. 9:2 NRHO in the Earth-Moon rotating frame (a); Accelerations acting on spacecraft in LLO and NRHO orbits (b).

Several investigations have already begun to explore orbit determination in the lunar NRHO regime. Newman et al. [5] perform a linear covariance analysis as a first look at NRHO navigation with Deep Space Network (DSN) tracking. Winternitz et al.[6] explore the enhancement in the OD solution available when a GPS receiver is included onboard, and Yun et al.[7] investigate adding optical measurements as well. Guinn et al.[8] investigate relative-only optical navigation strategies. Since the highly-nonlinear dynamics of this orbit challenge the assumptions underlying linear covariance

analyses, further analyses by Newman et al.[9] and Volle et al.[10,11] employ Monte Carlo OD simulations using both DSN and relative measurements.

The present work serves as a check to the assumptions of previous studies and an independent verification of those results. Various navigation trades are performed, including: tracking cadence, tracking pass placement, filter type, measurement noise, and measurement type. Spacecraft state uncertainty estimates are evaluated as a function of time. Simulated range and range-rate measurements with DSN ground stations are used to model orbit determination accuracy. Orbit maintenance maneuvers are performed using both short-horizon and long-horizon stationkeeping targeting. Finally, a Monte Carlo analysis of orbit determination and stationkeeping is performed.

II. Dynamics and Assumptions

Spacecraft dynamics are modeled in GMAT (the General Mission Analysis Tool, developed at Goddard Space Flight Center)[12] and Monte (Mission Analysis, Operations, and Navigation Toolkit Environment, developed at the Jet Propulsion Laboratory).[13] In this analysis, GMAT generates the "truth" solution with the following forces modeled:

- 32x32 spherical harmonics gravity field model of the Moon from the GRGM 900c model.
- Point masses of the Earth, Sun, and barycenters of all other planetary systems in the solar system, with states from the JPL DE430 ephemerides.[14]
- Solar radiation pressure (SRP) with a spherical spacecraft with coefficient of reflectivity of 1.3. Mass and surface area depend on the Gateway configuration according to Table 1. These values are representative of possible Gateway configurations.
- Relativistic correction.

The filter dynamics are slightly different from the "true" dynamics in order to represent realistic mis-modeling of small forces. Note that although the spherical model for SRP is not generally very accurate, it is a good approximation in this case. The Gateway is assumed to be oriented in SPEA (solar pressure equilibrium attitude), a sun-fixed attitude identified to minimize torques caused by SRP. Since this attitude is fixed relative to the Sun, using an equivalent area flat plate or spherical model captures the true dynamics accurately. The filter dynamics are implemented separately in GMAT and Monte and include the following forces:

- 16x16 spherical harmonics gravity field model of the Moon from the GRGM 900c model.
- Point masses of the Earth, Sun, and barycenters of all other planetary systems in the solar system, with states from the JPL DE430 ephemerides.[14]
- Solar radiation pressure with a spherical spacecraft. Mass, surface area, and coefficient of reflectivity are initialized randomly with error according to the uncertainties given in Table 2.
- Relativistic correction.

Navigation is simulated separately in GMAT and in Monte. In both navigation simulations, the filter defines the dynamics in an Earth-centered J2000 inertial reference frame. The GMAT simulation uses a batch filter iterated until convergence. Convergence is defined as meeting the absolute and relative weighted RMS convergence criteria (0.01 and 0.001, respectively) and usually takes 3-5 iterations. GMAT's outer loop sigma editing (OLSE) is not used here because the simulated measurements are known to all be valid. In real operations, outlier measurements would be ignored to avoid incorporating bad data.

The Monte simulation compares two different filters: the U-D factorized covariance filter, and the square root information filter (SRIF). Both of these filters are meant to mitigate the numerical instability of conventional Kalman filters as the covariance matrix becomes ill-conditioned.[15,16] The SRIF has been previously used in interplanetary spaceflight on Mariner 10, and showed key advantages over a conventional batch filter during Venus flyby, a key phase of the mission. The low perilune of an NRHO provides a dynamic environment somewhat comparable to a planetary flyby, and as such, these filters are likely well-suited for use in an NRHO. Both filters in Monte use stochastic accelerations on the order of 5×10^{-7} mm/s^2 updated every 8 hours to absorb dynamical mis-modeling.

In this analysis, a data arc always consists of nearly one complete orbit, starting immediately after the orbit maintenance maneuver (OMM) performed at apolune, and ending at the data cutoff 24 hours before the next apolune. Ground station tracking passes are allowed between apolune and data cutoff only. OMMs are not estimated. Future analysis will model the OMMs in the filter and also allow tracking passes during the 24 hours between data cutoff and the next apolune (these data would be used to estimate the state for the subsequent data cutoff).

All analyses in this paper use three DSN (Deep Space Network) ground stations, with a maximum of one ground station active at a time. The ground stations simulate a 35-m dish at the Madrid, Canberra, and Goldstone facilities. The Gateway performs tracking passes with the DSN on X-band radio. Measurement noise in reality is dependent on the signal to noise ratio of the communication link, which is in turn dependent on many factors, such as the ground radio specifications, spacecraft radio specifications, and weather in Earth's ionosphere.[17] The measurement noise

specified in Table 2 is chosen to be similar to the real measurement noise found from post-processing of the ARTEMIS mission[18] All maneuvers are assumed to be impulsive changes in velocity (ΔV).

As the Gateway is constructed element-by-element, there will be many different vehicle configurations, each with its own operational requirements. In the present analysis, only the first two potential configurations are examined: PPE (power & propulsion element) only, and PPE + HALO (Habitation and Logistics Outpost). In these configurations, Gateway is in a quiescent (uncrewed) state, which results in smaller and less frequent perturbations. With crew aboard, venting becomes a significant source of uncertainty in the dynamics. Later configurations also experience larger gravity gradient torques near perilune, requiring more frequent momentum wheel desaturation maneuvers. The present analysis assumes that a single desaturation maneuver is performed each orbit in a random direction, immediately before each OMM.

Table 1. Representative values for the Gateway configurations analyzed.

Gateway Configuration	*Mass [kg]*	*Sun-facing area [m^2]*
1) PPE	5700	310
2) PPE + HALO	13700	340

Table 2. Assumed sources of uncertainty.

Error source	*Uncertainty (3σ)*
Mass uncertainty	3%
SRP area	30%
Coefficient of reflectivity	45%
OMM execution error	1.42 mm/s fixed, 1.5% proportional, 1 deg pointing
Measurement bias	7.5 m (range), 2.5 mm/s (range-rate)
Measurement noise	3 m (range), 1 mm/s (range-rate)

Table 3. A priori state error and covariance.

Estimated parameter	*3σ a priori state error relative to truth (applied once at start of simulation)*	*a priori covariance (re-initialized at the start of every data arc)*
Position in Earth-centered J2000	10 km	∞ km
Velocity in Earth-centered J2000	10 cm/s	∞ m/s
Coefficient of reflectivity	45%	∞
Range measurement bias	1 m	∞
Range-rate measurement bias	1 mm/s	∞

III. Navigation Study Setup

The present work builds on results from the literature discussed above to outline the operational requirements for NRHO navigation. Typical statistical orbit determination relies on two fundamental assumptions:

1) The spacecraft state uncertainty distribution is always Gaussian.
2) The state dynamics and measurement-state relationships can be linearized relative to a reference trajectory.

In an NRHO, both of these assumptions are pushed to their limits. Figure 2 shows how the standard moments (standard deviation, skewness, and excess kurtosis) evolve over time, for an initial 3σ covariance of 10 km position in each axis and 10 cm/s velocity in each axis, sampled at apolune. The values in Figure 2 are computed based on a Monte Carlo simulation with 1,000 samples. Even over a single orbit, the dynamics are clearly nonlinear, and the state uncertainty quickly becomes non-Gaussian.

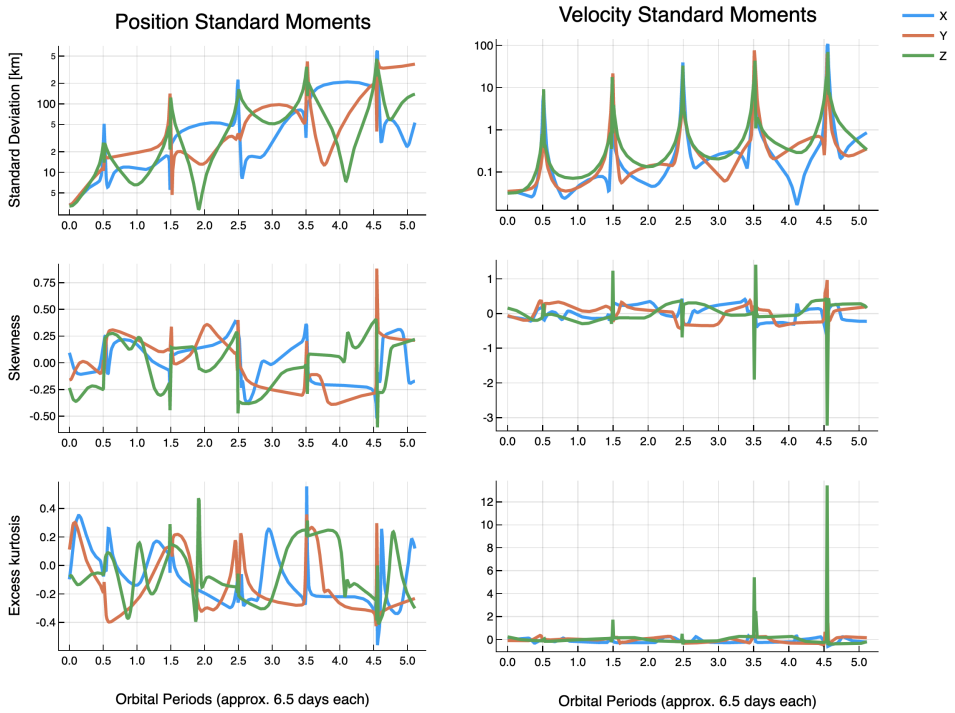

Figure 2. Evolution of position and velocity standard moments over time in an NRHO.

Linear covariance analysis is a common way to approximate spacecraft navigation performance. A covariance analysis, also known as a Cramer-Rao analysis,[19] is essentially equivalent to a single iteration of a sequential filter. The update to the covariance matrix is computed with each measurement, but the measurement is not used to update the state estimate. Covariance analysis is adequate when the fundamental assumptions described above are satisfied or nearly satisfied. However, covariance analysis on its own can be misleading. For instance, it is entirely possible that a navigation filter would saturate and converge on an incorrect solution. Stochastic acceleration may be required in a real filter to capture significant but difficult-to-model forces. Engineering intuition is required to ensure that the covariance analysis does not return overly-optimistic results. Given the highly-nonlinear dynamics in an NRHO, it is not immediately obvious to what extent linear covariance analysis can be trusted in this regime. The goal of the present analysis is to set up a realistic navigation analysis which makes the fewest assumptions possible, then quantify the navigation performance for various operations parameters.

The navigation simulation uses three spacecraft: the Reference, which is an idealized target; the Truth, which simulates the real spacecraft; and the Navigation spacecraft, which represents the best estimate of the Truth at any time. Figure 3 illustrates the role each of these spacecraft play in the simulation. The filter never knows the state of the Truth directly. Simulated range and range-rate measurements are generated (with noise and bias errors) from the Truth and subsequently passed through the filter, as shown in Figure 4.

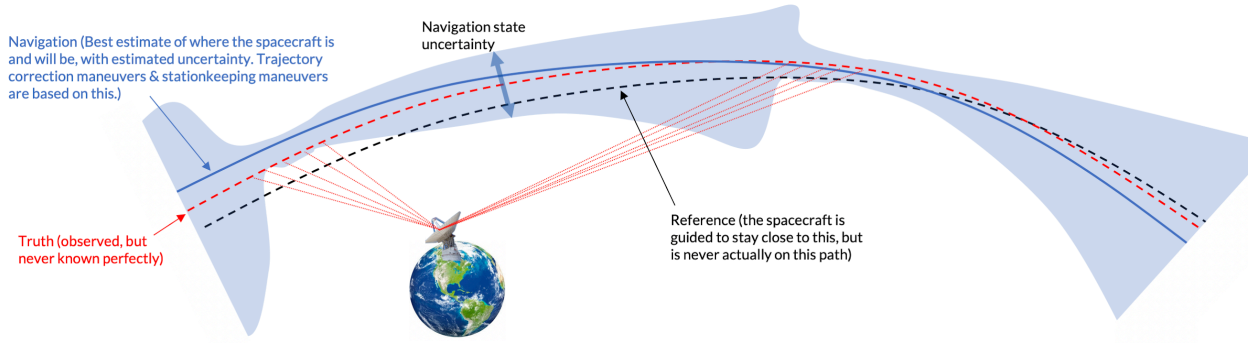

Figure 3. Conceptual diagram of the relationship between the Reference, Navigation, and Truth spacecraft.

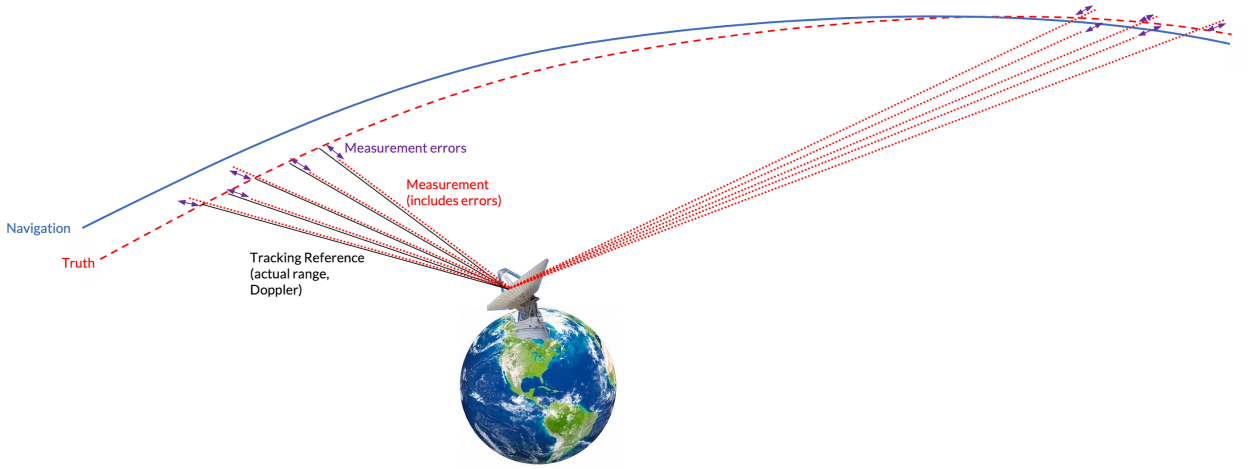

Figure 4. Conceptual diagram of measurement errors.

In multi-body dynamics, results in the literature have shown that the navigation state accuracy is closely correlated to mission ΔV.[20] The present results agree with that finding. Figure 5 shows a conceptual diagram of why that is the case. Trajectory correction maneuvers (TCMs) or orbit maintenance maneuvers (OMMs) are always designed based on the Navigation spacecraft — the best estimate of the Truth state. In general, there will always be some error between the Navigation state and the Truth state at the maneuver execution epoch. This error is exacerbated by a simple practical concern: the maneuver must be designed based on data available as of the data cutoff epoch, which is assumed here to be 24 hours before the maneuver execution epoch. Between the data cutoff epoch and the maneuver execution epoch, the ground-based navigation team must carry out a series of important analyses: process the measurement data to-date, design a nominal maneuver, ensure that the maneuver execution error will not endanger the mission, build the spacecraft instructions, and upload the instructions to the spacecraft. A good example of this process is described in the experience from the Dawn mission.[21]

While these ground-based operations are taking place, the Navigation state uncertainty grows. When the maneuver is executed, it is based on an incorrect state estimate and executed with error. If these errors are small, they do not contribute much to the total ΔV of the mission. However, the chaotic nature of multi-body dynamics means that real errors have a significant effect on the mission. In a navigation simulation, care must be given to represent these constraints and errors realistically.

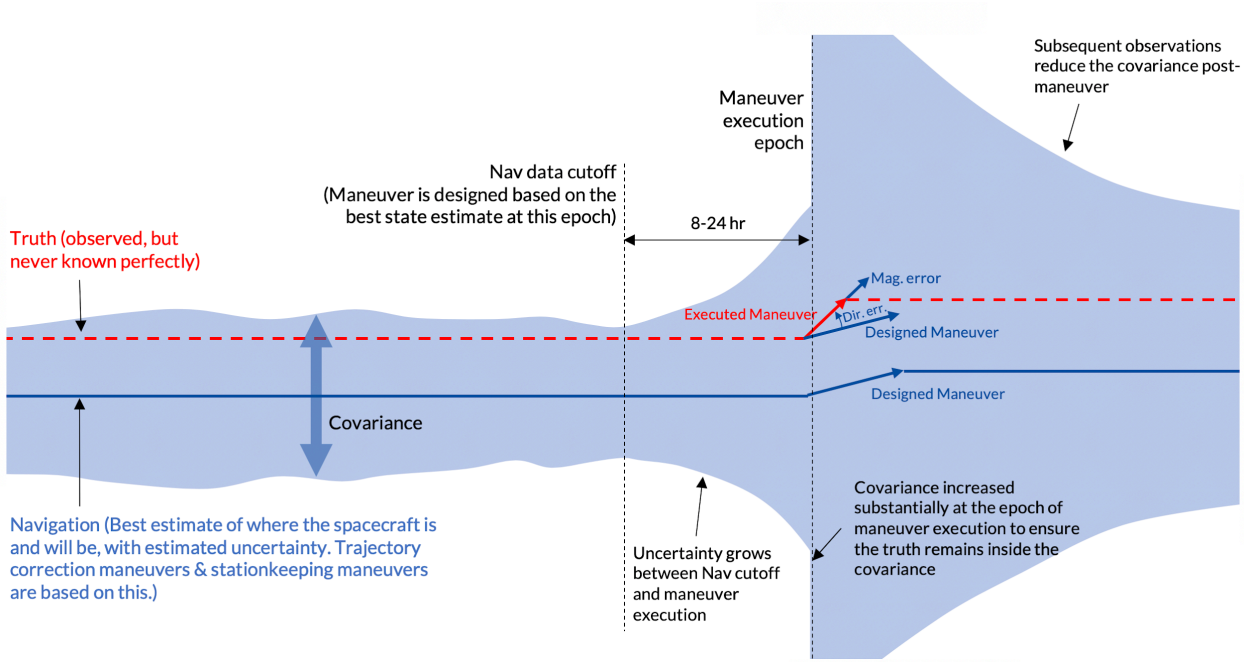

Figure 5. Conceptual diagram of navigation errors and uncertainty.

In order to preserve the validity of the results of a simulated navigation study, it is important that the navigation estimate never directly touches the truth. Or, in other words, the navigation simulation must not cheat by having unrealistic knowledge of the truth. This concept is visualized in Figure 6. The present analysis goes to lengths to ensure that the Truth and Navigation spacecraft are isolated from each other. This is done by modeling them in different software (Truth in GMAT, Navigation in Monte), using different force models, and using realistic a priori state error and covariance in the filter.

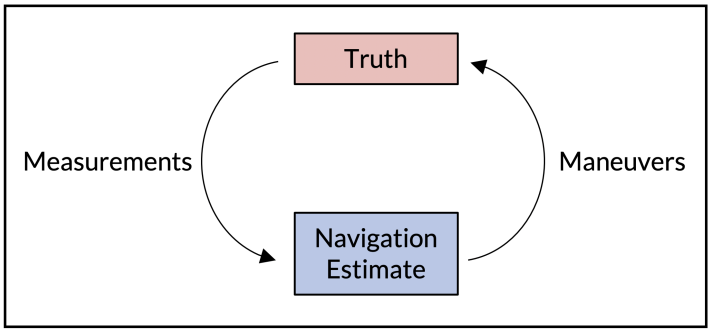

Figure 6. Conceptual relationship between truth and the navigation estimate.

One common metric for filter performance is the covariance at the end of a data arc. However, as noted above, the covariance alone is not a sufficient metric. In the present analysis, filter performance is judged based on the following characteristics, in addition to the covariance:

- Convergence or divergence.
- Truth trajectory remaining within the uncertainty bounds of the navigation solution.
- Accuracy of the navigation solution (relative to truth).
- The ability of the truth spacecraft to efficiently and safely maintain its orbit while executing maneuvers designed based on the navigation solution.

IV. Results

The results in this section describe analyses of NRHO insertion cleanup, stationkeeping, and navigation trades—all with simulated orbit determination.

A. NRHO Insertion

Because the NRHO Insertion Maneuver (NIM) is modeled to occur at perilune, an area known to be very dynamically sensitive, a pair of post-insertion maneuvers is designed to bring the resulting trajectory closer to the reference. The strategy for these maneuvers is based on the long-horizon orbit maintenance strategy described by Davis et. al.[22] The Insertion Correction Maneuver (ICM) strategy is depicted in Figure 7. ICM-1 targets the position of the reference orbit at the epoch of ICM-2. After ICM-1 is performed, the spacecraft coasts to ICM-2, where it targets velocity continuity with the reference at the same epoch. This maneuver is not applied, however, and instead is used as the initial guess for an OMM, which is performed in place of ICM-2. The standard OMM procedure is described in Section IV B.

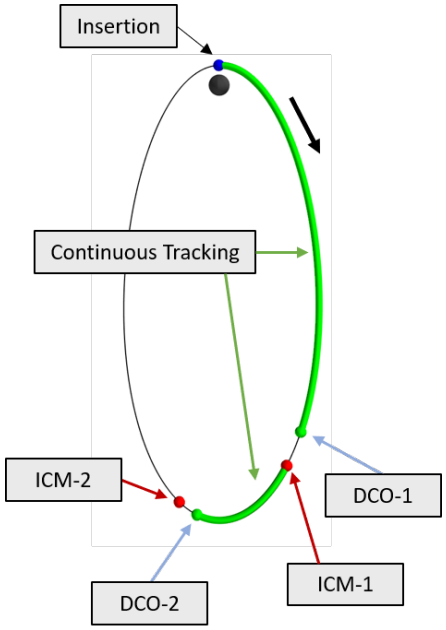

Figure 7. Conceptual diagram of the Insertion Correction Maneuvers strategy.

For this analysis, it is assumed that there is continuous tracking between insertion and the first data cutoff point, labelled DCO-1 in Figure 7, as well as between ICM-1 and DCO-2. Trades in the elapsed time between each of DCO points and maneuver execution times, as well as the temporal spacing of the maneuvers, are all considered. The trades are summarized in Table 4. Each case represents a Monte Carlo analysis of approximately 100 runs, each sampling random errors for insertion, desaturation perturbations, and OMM execution. The insertion errors were determined by sampling errors from the NRHO insertion maneuver (NIM) of a ballistic lunar transfer (BLT). The navigation requirements and expected performance are studied in a parallel analysis in Parrish et al.[23]

Table 4. Summary of Insertion Correction Maneuver trades. *Note that true anomaly is undefined for three-body orbits, but the osculating true anomaly serves as a useful metric for position within the orbit. See Phillips et al.*[24] *for a depiction of osculating true anomaly in the context of a 9:2 NRHO.*

	Event Separation				Event True Anomaly (Osculating) [degrees]			
Case	**NIM to DCO-1**	**DCO-1 to ICM-1**	**ICM-1 to DCO-2**	**DCO-2 to ICM-2**	**DCO-1**	**ICM-1**	**DCO-2**	**ICM-2**
1	1 day	8 hours	2 days	1 day	158	163	181	189
2	2 days	8 hours	2 days	1 day	170	173	189	201
3	2 days	1 day	2 days	1 day	170	179	196	217

The results for each case are presented in Table 5. In all cases, ICM-1 contributes a majority of the total ΔV, with ICM-2 often possessing a maneuver that is an order of magnitude smaller. The results indicate that ICMs performed closer to perilune result in a smaller total ΔV, but a greater separation between the maneuvers does not correspond to a lower ΔV. While it is clear from the results that the spacing of the maneuvers has a large impact on the total cost, it is not necessarily true that Case 1 is an optimal solution, as this trade space was small. Again, it appears that maneuvers performed closer to perilune offer greater fuel savings, but more analysis is required to identify the best location; an ICM performed very close to perilune might yield a low initial cost, but the sensitivity of the NRHO around perilune may result in a higher total ΔV and/or a trajectory that is still very far from the reference due to maneuver execution errors and other perturbations. Future analysis will explore this trade more thoroughly.

Table 5. Summary of ICM results.

Case	**ICM-1 Cost [m/s]**		**ICM-2 Cost [m/s]**		**Total ICM Cost [m/s]**				
	Mean	**STD**	**Mean**	**STD**	**Min**	**Max**	**Mean**	**STD**	**DV99**
1	1.879	1.380	0.431	0.307	0.056	9.053	2.311	1.682	7.589
2	2.839	2.158	0.784	0.581	0.094	15.10	3.623	2.735	12.024
3	3.934	2.964	1.125	0.822	0.106	19.721	5.059	3.782	16.308

B. Stationkeeping

This analysis implements both a short-horizon and a long-horizon stationkeeping strategy, with state estimation updates provided by a navigation filter processing simulated observations. The short-horizon algorithm is designed to keep the spacecraft in the vicinity of the NRHO without applying stringent, high-ΔV constraints. The long-horizon strategy is applied to maintain the phase of the NRHO; that is, to ensure the perilune passage time of the Gateway does not drift far from that of the reference NRHO. The goal is to avoid long eclipses from the Earth's shadow, which are absent from the reference,[25] and also to provide a predictable state for spacecraft arriving and departing from the Gateway. The predictable timing of the Gateway state within the NRHO will facilitate transfers to and from Earth as well as lander missions to the lunar surface.

The short-horizon stationkeeping strategy implemented in the current study is an x-axis crossing control scheme. A maneuver at apolune is designed to target the x-component of rotating velocity, v_x, along a reference trajectory at perilune 6.5 revolutions downstream. This strategy has been found effective in literature.[9,26] OMMs with magnitudes under 3 cm/s are not executed for the sake of operational simplicity.

Stationkeeping ΔV as a function of Gateway configuration

Different configurations of the Gateway have different physical properties. An important parameter that affects stationkeeping cost is the vehicle's area-to-mass ratio (AMR), which influences the magnitude of SRP perturbations. This is especially important when targeting the 15-year reference NRHO, which does not include SRP forces. To illustrate this effect, two configurations of the Gateway, PPE vs PPE+HALO are simulated in the NRHO for one year with a consistent tracking schedule of 8 hours per day. The only differences between the simulations are the area and mass properties of the vehicle. Note that these cases did not implement any long-horizon stationkeeping maneuvers, and the OMM fixed execution error is larger than what is listed in Table 2 at 9 mm/s. The results are listed in Table 6. The second configuration, with the lower area-to-mass ratio, results in an annual stationkeeping cost that is approximately half that of the higher AMR case. The standard deviation of both cases is similar, though, which indicates that the area-to-mass ratio in this range does not significantly impact the spread of maneuver magnitudes.

Table 6 Stationkeeping cost as a function of Gateway configuration.

Gateway Configuration	Mean Annual ΔV[m/s]	Annual ΔV 1σ [m/s]
PPE	4.43	0.58
PPE + HALO	2.42	0.51

Comparison of long-horizon SK implementation options

This analysis implements an alternative long horizon stationkeeping strategy, depicted in Figure 8. The strategy is similar to that of Davis et al.[22] with some minor modifications, most notably with regard to the timing of the maneuvers along the orbit: both of the long-horizon maneuvers are performed at apolune. The first maneuver, which occurs at time t_0, targets the position vector and the apolune epoch of the reference NRHO one revolution downstream, at time t_1. The resulting post-maneuver state is propagated for one revolution, to t_1, at which time the second long-horizon maneuver is designed. This second maneuver simply achieves velocity continuity with the reference at t_1.

Upon reaching t_1, there are two feasible options. The first option performs the second maneuver as designed (subject to maneuver execution errors). The second option does not perform that maneuver, but instead uses it as the initial guess for an OMM that occurs at t_1, according to the short horizon stationkeeping strategy. Both options are effective strategies for long-term maintenance of the NRHO, as both implementations are found to safely maintain the NRHO for at least one year. However, the first option achieves an orbit that is closer to the reference, as it targets the full 7-state (position, velocity, and time). Because of these extra constraints, though, this option results in higher-ΔV long-horizon maneuvers than the second option. It is possible that the first option, though more expensive, may prove necessary for multi-year stationkeeping—such an investigation is outside the scope of this analysis, however. A comparison of these strategies is presented in Table 7.

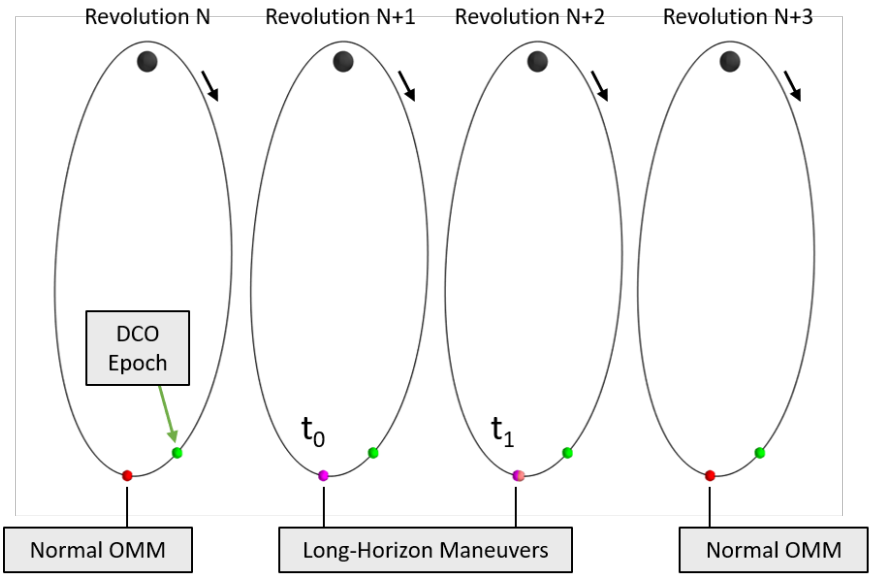

Figure 8. Conceptual diagram of the apolune-to-apolune long-horizon stationkeeping strategy.

Cases 1 & 2 use a batch filter on simulated range and range-rate data. Cases 3–6 approximate navigation by perturbing the "navigation" spacecraft relative to the "truth" spacecraft prior to performing the maneuver. Cases 1–4 use the second apolune-to-apolune long-horizon maneuver option (using the long-horizon maneuver at t_1 as the initial guess for an OMM), while cases 5-6 use the first apolune-to-apolune option (implementing the long-horizon maneuver as designed).

The first noteworthy comparison is between cases 3–4 and cases 5–6, which shows that the second long-horizon options produced maneuvers that are almost half the DV cost as compared to the first option. The second noteworthy comparison is between cases 1–2 and cases 3–4, which shows that the results generated using simulated DSN measurements produced a smaller annual cost. This is expected, as the state uncertainties returned from the 8-hours-per-day cadence are almost always smaller than the state uncertainties sampled for the navigation perturbations in cases 3–6. Finally, in all cases, more frequent long-horizon maneuvers resulted in higher annual costs, but the change was not dramatic.

Table 7. Results of Monte Carlo trials of apolune-to-apolune stationkeeping strategy.

Case	Long-Horizon Frequency [# of orbits]	3σ State Uncertainties [km, cm/s]	Mean Annual ΔV [m/s]
1	10	N/A (8hr / day tracking)	4.273 ± 2.061
2	15	N/A (8hr / day tracking)	4.050 ± 2.093
3	10	10, 10	7.141 ± 1.048
4	15	10, 10	6.856 ± 1.169
5	10	10, 10	12.434 ± 3.046
6	15	10, 10	11.51 ± 2.50

Figures 9-11 show the results of a Monte Carlo analysis with 100 random trials for Case 1. The results shown here are for Gateway configuration #1 (PPE only, no crew). Figure 9 shows the OMMs as performed. Note that most maneuvers are approximately 5-10 cm/s, but every 10 revolutions, a pair of larger maneuvers of approximately 50

cm/s each are performed. The small maneuvers are the short-horizon OMMs, and the large ΔVs correspond to the long-horizon maneuvers.

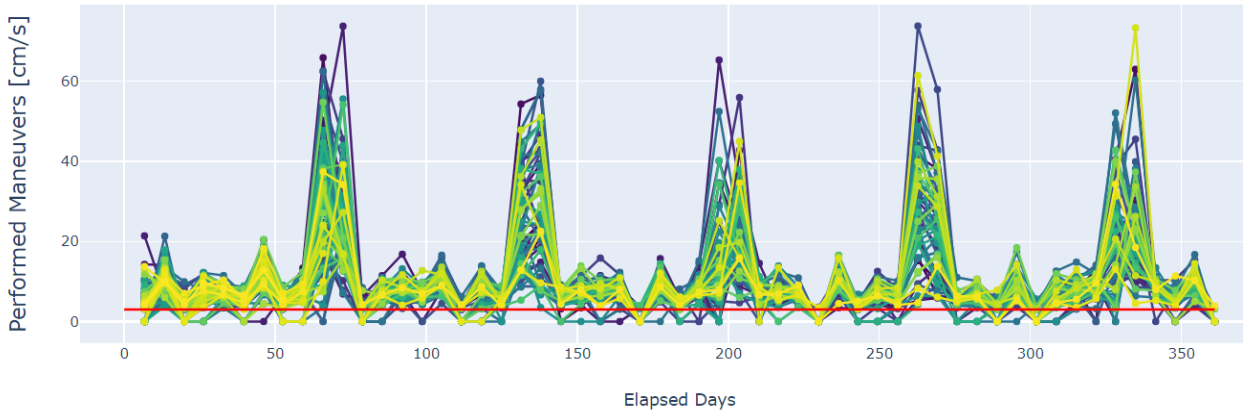

Figure 9. Stationkeeping maneuver magnitudes as performed.

Figure 10 shows the 1σ position and velocity covariance returned by a batch filter once per revolution at the data cutoff (24 hours before maneuver execution). The geometry and ground tracking for all the random trials is very similar, so the covariance results do not vary significantly from trial to trial. It is observed that following some of the long-horizon maneuvers, the state uncertainty is significantly larger than on the other revolutions. It is hypothesized that these come as a result of long-horizon maneuvers which happen to be aligned with the unstable eigenvector of the NRHO, but additional testing is required to understand the phenomena better. Further, the larger maneuvers necessarily result in larger execution errors. For the given tracking schedule, the state uncertainties are comparable to those found by past studies. This result implies that the general findings of covariance analyses are valid despite the nonlinearity of the problem. However, outliers are common, and further study is required to verify.

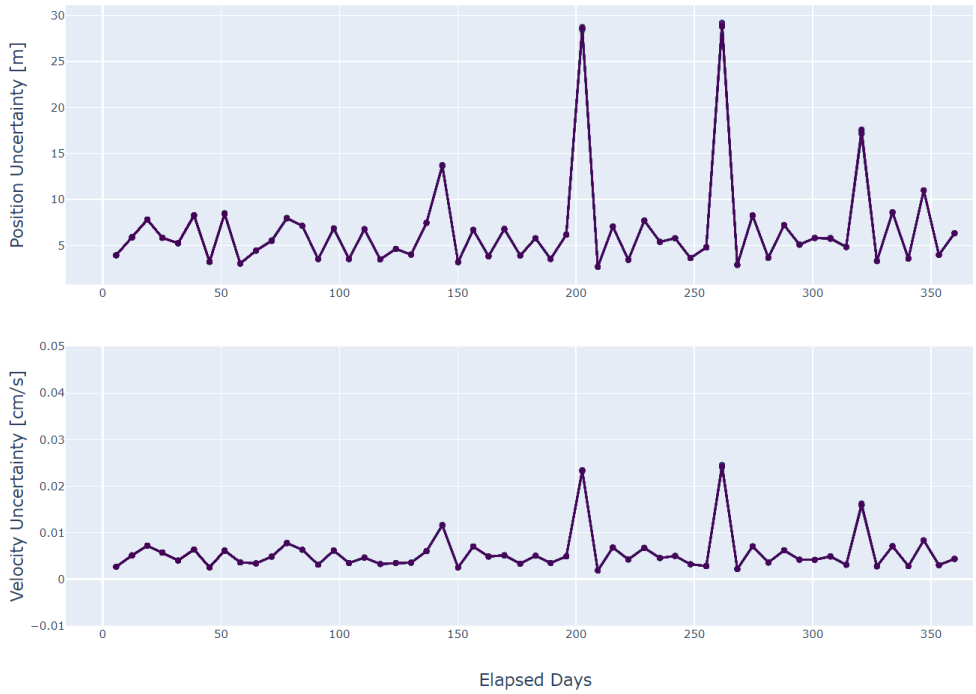

Figure 10. State uncertainty at each estimation epoch, with one eight-hour tracking pass per day.

Figure 11 shows the state error for each random trial immediately following each stationkeeping maneuver execution. The position errors are slightly larger than the uncertainties reported above, which is consistent with the uncertainty growing over the 24 hours between data cutoff and maneuver execution. The velocity error is substantially

larger because of the ~3 cm/s desaturation maneuver performed immediately before the OMM and because of the OMM execution error.

Figure 11. State error relative to truth immediately after each maneuver execution.

C. Navigation Trades

Several trades are presented to discuss the impact on navigation filter performance from tracking cadence, tracking pass phasing (where in the orbit the tracking passes take place), filter type, measurement noise, and measurement type.

Comparison of tracking cadence

For this analysis, a number of tracking cadences are evaluated with the U-D factorized covariance filter:

- Continuous
- 8 hours per pass, 7 passes per week
- 8 hours per pass, 3 passes per week
- 8 hours per pass, 2 passes per week
- 2 hours per pass, 7 passes per week
- 2 hours per pass, 3 passes per week
- 2 hours per pass, 2 passes per week

Table 8. Position and velocity 1σ uncertainties as a function of tracking cadence with U-D factorized covariance filter.

Tracking Cadence	Apolune Position Uncertainty [km]	Apolune Velocity Uncertainty [m/s]
Continuous	6.57×10^{-3}	6.65×10^{-5}
8 hours 7/week	1.91×10^{-2}	1.31×10^{-4}
8 hours 3/week	1.68×10^{-1}	8.85×10^{-4}
8 hours 2/week	7.80×10^{-2}	1.58×10^{-3}

2 hours 7/week	2.48×10^{-2}	1.65×10^{-4}
2 hours 3/week	4.40×10^{-2}	2.25×10^{-4}
2 hours 2/week	5.26×10^{-2}	1.24×10^{-3}

Interestingly, the "8 hours 3/week" case performs worse here than the "8 hours 2/week" case in terms of position uncertainty, but still shows a smaller velocity uncertainty. This is because of where the tracking passes happen to fall in the orbit. This analysis schedules tracking passes on a temporal basis alone, without any regard as to Gateway's phasing in the NRHO. For short data arcs like an NRHO revolution, the placement of tracking arcs with respect to the desired state can be more important than your cumulative tracking time.

Comparison of tracking pass phasing

A basic test to demonstrate the importance of where measurements are taken in the NRHO can be seen by analyzing the instantaneous estimated uncertainty during a continuous tracking cadence. A plot showing this uncertainty is shown in Figure 12. The data arc begins at one apolune and ends at the next apolune, with perilune marked.

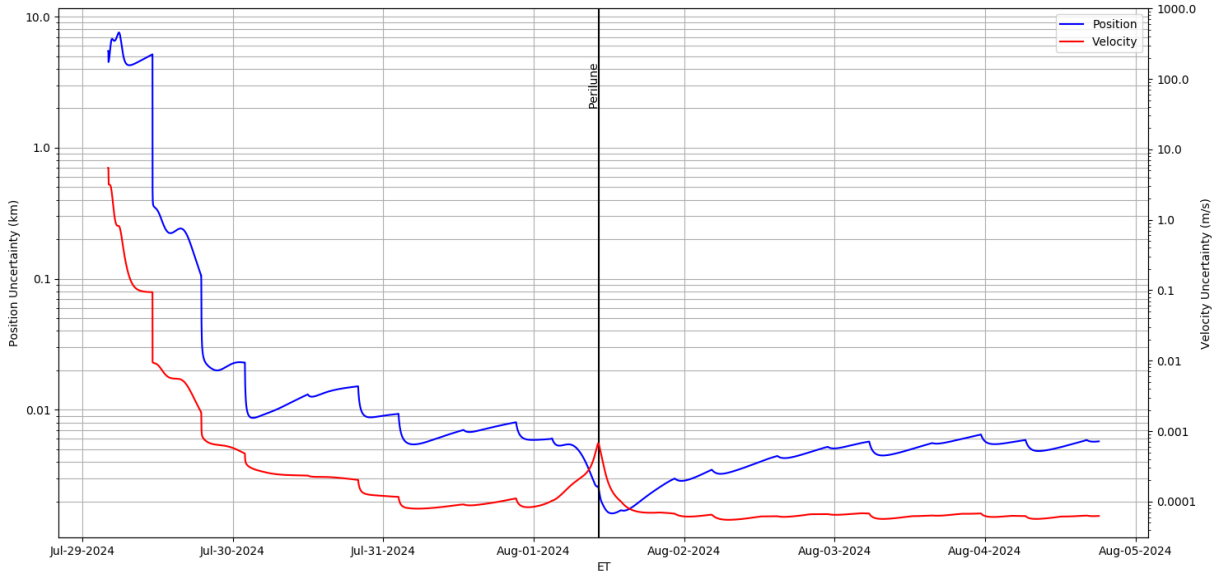

Figure 12. Position and velocity 1σ covariance magnitudes over one NRHO revolution with continuous tracking.

At perilune, the system is the most observable because the spacecraft traverses a large distance in a short time. As a result, the position covariance reaches its minimum at perilune. However, the difference between the gravity field used in the Truth and Navigation models becomes most apparent at perilune. The assumption that the dynamics are linearizable also breaks down the most at perilune. As a result of these effects, the velocity uncertainty is at a local maximum at perilune. It is not immediately obvious whether the improved observability or the degraded linearizability has the greater net effect.

Additionally, despite continuous tracking through the entire orbit, a spike in velocity uncertainty still occurs as the spacecraft passes through perilune. Figure 13 shows prefit and postfit Doppler residuals (in X-band Hz) of the simulated measurements. The uncertainty spike in velocity at perilune highlights the sensitivity of the dynamics, and in particular reveals that the filter has a hard time modeling the epoch of perilune. A slight state error at apolune corresponds to a large error at perilune, and a slight state error at perilune corresponds to a large error at apolune.

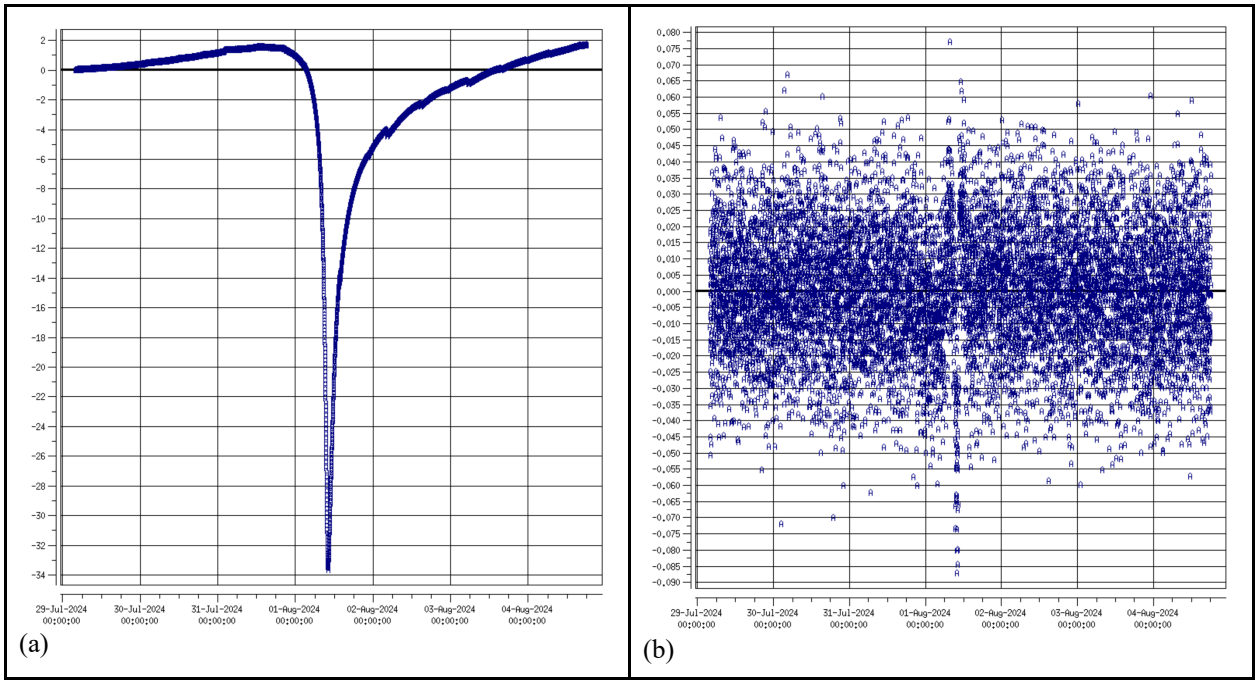

Figure 13. Prefit (a) and postfit (b) Doppler residuals (X-band Hz) over one NRHO revolution with continuous tracking.

Despite showing improvement over the a priori guess of the state, there are still clear artifacts of the chaotic dynamics at perilune, which leads to a spike in the velocity uncertainty. For this continuous tracking case, the spike is short lived, as new observations quickly correct the residuals. However, for cases where a tracking pass begins or ends at perilune, the filter may be thrown off by the fast dynamics. This has implications for spacecraft operations: an object deployed at or near perilune will have a large state uncertainty, and may prove troublesome for filter convergence.

Comparison of filter type

For this analysis, there are three tracking cadences used to compare the filter performance between GMAT and Monte. Each of the cadences uses a combination of three predefined tracking windows. The three tracking cadences are each 8 hours in duration, spaced about the NRHO in approximately-equal intervals. They are depicted in Figure 14. The first pass begins 1 day after apolune, the second pass begins 3 days after apolune, and the third pass begins 8 hours before DCO. The first analysis case uses only pass #3, the second case uses passes #1 and #3, and the third case uses all three passes.

In addition to the GMAT and Monte filter performance comparison, each case was simulated for one year with 100 random samples using with the GMAT batch filter. The results of each case are presented in Table 9. The columns under the header "All" represent the results of all attempted orbit determination events, including those for which the filter did not converge—hence the large covariances. The columns under the header "Converged Only" consider only the orbit determination events for which the filter converged, and the metric "Filter Convergence" represents the number of successfully converged orbit determination events (each event corresponds to one revolution of the NRHO). Because the tracking cadences are quite sparse, it is unsurprising that there is a relatively high number of unconverged events. The state errors are evaluated by comparing the estimated state to the state of the truth spacecraft at the same epoch. Such a comparison is impossible in actual operations, as the state of the truth spacecraft is never known, but this is one useful metric of identifying if the filter is trustworthy; state errors that are within some bound of the covariance—1-sigma in this example—indicate that the filter is converging on a realistic solution.

As expected, more frequent tracking yields a higher convergence percentage, as well as smaller covariances and state errors. The single-pass case exhibits the worst performance in all metrics, with the other cases providing improvements by at least one order of magnitude. Further, the mean state errors from the "Pass 3 only" case are larger than the corresponding 1-sigma covariance, while the mean state errors in the other two cases are smaller than their corresponding 1-sigma covariances. Note that this does not necessarily mean that the first case yields an unusable solution, only that the other cases are producing more trustworthy solutions.

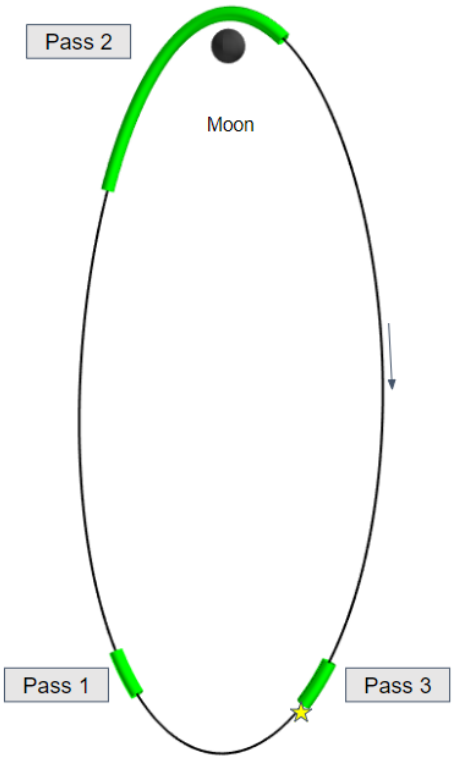

Figure 14. Three tracking windows used for comparison.

Table 9. Comparison of GMAT batch filter performance for different tracking cadences.

Case	All		Converged Only		
	Filter Convergence	**Mean 1σ Covariance [km, m/s]**	**Mean 1σ Covariance [km, m/s]**	**Mean State Error [km, m/s]**	**State Error Standard Deviation [km, m/s]**
Pass 3 only	65%	125.74, 2.144	8.819, 0.055	10.094, 0.0680	219.24, 0.4803
Passes 1 and 3	90%	0.1058, 7.119×10^{-4}	0.0809, 6.409×10^{-4}	0.0604, 4.446×10^{-4}	0.0670, 3.865×10^{-4}
Passes 1, 2, and 3	99%	0.0186, 1.149×10^{-4}	0.0185, 1.148×10^{-4}	0.0150, 9.435×10^{-5}	0.0153, 9.117×10^{-5}

The batch filter is then compared directly to the U-D Factorized Covariance filter and the Square Root Information Filter (SRIF), for a single revolution in the NRHO. The same Truth spacecraft is used in both GMAT and Monte. The two pieces of software generate simulated measurements separately, with the same measurement noise and tracking passes. Results of the comparison are shown in Table 10. As expected, all three filters find that increasing the number of tracking passes per revolution improves filter performance. The U-D Factorized Covariance filter and the SRIF both return exactly the same covariance, which is different than the value returned by the GMAT batch filter. In the first two cases, the GMAT batch filter yielded worse performance, but in the final case, the batch filter yielded the best performance (noting that all the covariances are on the same order of magnitude for this case).

Table 10. Comparison of filter types and tracking cadences over a single data arc.

Case	1σ uncertainty, GMAT Batch	1σ uncertainty, Monte U-D Factorized Covariance	1σ uncertainty, Monte SRIF
Pass 3 only	5.641 km, 0.120 m/s	1.836 km, 0.0175 m/s	1.836 km, 0.0175 m/s
Pass 1 & 3	0.306 km, 0.00351 m/s	0.040 km, 0.00083 m/s	0.040 km, 0.00083 m/s
Pass 1, 2, & 3 (nominal)	0.016 km, 0.00009 m/s	0.025 km, 0.00016 m/s	0.025 km, 0.00016 m/s

Comparison of measurement noise

In this analysis, the impact of measurement noise is considered for the case where three tracking passes are used per orbit, as described above. The U-D factorized covariance filter in Monte is used. Filter performance is reported as covariance at the end of a representative data arc (apolune 24 hours after data cut-off). Results are shown in Table 11.

Table 11. Position and velocity 1σ uncertainties as a function of measurement noise with U-D factorized covariance filter.

Measurement noise (3σ)	Apolune Position Uncertainty [km]	Apolune Velocity Uncertainty [m/s]
3 m, 1 mm/s (nominal)	2.49×10^{-2}	1.60×10^{-4}
10 m, 10 mm/s	3.39×10^{-2}	2.06×10^{-4}
15 m, 25 mm/s	3.92×10^{-2}	2.38×10^{-4}

Comparison of measurement type

In this analysis, the impact of measurement type is considered for the case where three tracking passes are used per orbit, as described above. Range-only, range-rate-only, and range plus range-rate data types are considered with the U-D factorized covariance filter. Range measurements require more communications bandwidth than Doppler measurements, so it would be useful if spacecraft could perform reasonable navigation on Doppler alone, particularly for spacecraft with small antennas. Filter performance is reported as covariance at the end of a representative data arc (apolune 24 hours after data cut-off). Results are shown in Table 12. Note that the uncertainty is smaller for the case with range data only than the case with range and range-rate data. This is most likely because the filter struggles to fit velocity through perilune (as observed in Figs 13-14). However, the highly-nonlinear behavior near perilune is real. The filter with range data only is likely returning an overly-optimistic estimate of the state uncertainty. This reveals one of the limitations of relying completely on covariance to determine filter performance.

Table 12. Position and velocity 1σ uncertainties as a function of measurement type with U-D factorized covariance filter.

Measurement type	Apolune Position Uncertainty [km]	Apolune Velocity Uncertainty [m/s]
Range only	1.91×10^{-2}	1.32×10^{-4}
Range-rate only	6.60×10^{-2}	3.56×10^{-4}
Range + range-rate (nominal)	2.49×10^{-2}	1.60×10^{-4}

V. Conclusion

The analyses in this paper address a range of questions related to operating a spacecraft in an NRHO. These results can inform requirements for flight. Various trades on NRHO insertion cleanup, short-horizon, and long-horizon stationkeeping were performed. Realistic options are considered for tracking cadence, tracking measurement noise, and tracking pass phasing.

It was found that a two-maneuver strategy can successfully clean up errors associated with NRHO insertion, which often occurs in an area that is highly dynamically sensitive. The cost of insertion cleanup varies with the location of the maneuvers, with the total cleanup cost ranging from 0.056 m/s to over 16 m/s. It was shown that the area-to-mass ratio of a spacecraft in an NRHO has a large impact on the annual stationkeeping cost due to SRP perturbations. Further, various implementations of long-horizon stationkeeping maneuvers can produce significantly lower or higher annual costs.

It was found that the phasing tracking passes within the NRHO can be more important than the cumulative tracking time, partially due to the significant nonlinearities associated with region around perilune. Various tracking cadences were implemented to compare the delivered state uncertainties and filter performance. Different filters were also applied to these cadences. Finally, trades in measurement noise and measurement types were studied to compare the filter performance.

Future work will consider additional combinations of the various trades presented here. NASA and Advanced Space will demonstrate NRHO navigation and operation with the CAPSTONE mission, currently planned for launch in December 2020.

The authors wish to acknowledge support from the NASA SBIR (Small Business Innovative Research) program for funding, and Caltech for the use of Monte software.

References

1. Whitley R, Martinez R. Options for staging orbits in cislunar space. In: *IEEE Aerospace Conference Proceedings*. ; 2016. doi:10.1109/AERO.2016.7500635
2. Dunham DW, Farquhar RW. Libration Point Missions, 1978 – 2002. *Libr Point Orbits Appl - Proc Conf Aiguablava Spain 10-14 June 2002*. 2003:45-73. doi:10.1142/9789812704849_0003
3. Bosanac N, Webster CM, Howell KC, Folta DC. Trajectory design and station-keeping analysis for the wide field infrared survey telescope mission. In: *Advances in the Astronautical Sciences*. ; 2018.
4. Woodard M, Cosgrove D, Morinelli P, Marchese J, Owens B, Folta D. Orbit determination of spacecraft in Earth-Moon L1 and L2 libration point orbits. *Adv Astronaut Sci*. 2012;142:1683-1696.
5. Newman CP, Davis DC, Whitley RJ, Guinn JR, Ryne MS. Stationkeeping, Orbit Determination, and Attitude Control for Spacecraft in Near Rectilinear Halo Orbits. *AAS/AIAA Astrodyn Spec Conf*. 2018:1-20.
6. Winternitz LB, Goddard N, Flight S, et al. GPS Based Autonomous Navigation Study for the Lunar Gateway. *Aas*. 2019:1-16.
7. Yun S, Zanetti R, D'Souza CN. Sensor Configuration Trade Study for Navigation in Near Rectilinear Halo Orbits. In: *AAS/AIAA Astrodynamics Specialist Conference*. Portland, ME; 2019.
8. Guinn JR, Bhaskaran S, Ely TA, et al. The Deep Space Positioning System (DPS) Navigator Concept for the Lunar Gateway. In: *42nd Annual AAS Guidance and Control Conference*. Breckenridge, CO; 2019.
9. Newman CP, Sieling R, Davis DC, Whitley RJ. Attitude Control and Orbit Determination of a Crewed Spacecraft With Lunar Lander in Near Rectilinear Halo Orbit. In: *AAS/AIAA Astrodynamics Specialist Conference*. Ka'anapali, HI; 2019.
10. Volle MJ. Distant Retrograde Orbit Constellations for Relative-only Navigation in Near Rectilinear Halo Orbits. In: *AAS/AIAA Space Flight Mechanics Meeting*. Ka'anapali, HI; 2019.
11. Volle MJ, Davis DC. Examining the feasibility of relative-only navigation for crewed missions to near rectilinear halo orbits. *Adv Astronaut Sci*. 2018;167:3833-3852.
12. Jah M, Hughes S, Wilkins M, Kelecy T. The general mission analysis tool (GMAT): A new resource for supporting debris orbit determination, tracking and analysis. In: *European Space Agency, (Special Publication) ESA SP*. ; 2009.
13. Jonathon Smith W. MONTE Python for Deep Space Navigation. *Proc 15th Python Sci Conf*. 2016;(Scipy):62-68. doi:10.25080/majora-629e541a-009
14. Folkner WM, Williams JG, Boggs DH, Park RS, Kuchynka P. *The Planetary and Lunar Ephemerides DE430 and DE431*. Vol 196.; 2014.
15. Thornton CL. *Triangular Covariance Factorizations for Kalman Filtering*.; 1976.
16. Bierman GJ. Sequential square root filtering and smoothing of discrete linear systems. *Automatica*.

1974;10(2):147-158. doi:10.1016/0005-1098(74)90020-X
17. Gamper E, Kebschull C, Stoll E. Statistical Orbit Determination using the Ensemble Kalman Filter. *Acta Astronaut*. 2018;(January):22-24.
18. Leonard JM, Cheetham BW, Born GH. Preliminary Evaluation of Earth-Moon Libration Point Orbit Navigation with Post-Processed ARTEMIS Data. In: *24th International Symposium on Space Flight Dynamics*. Laurel, MD; 2014.
19. Taylor JH. The cramér-rao estimation error lower bound computation for deterministic nonlinear systems. In: *Bayesian Bounds for Parameter Estimation and Nonlinear Filtering/Tracking*. ; 2007. doi:10.1109/9780470544198.ch65
20. Howell KC, Gordon SC. Orbit determination error analysis and a station-keeping strategy for sun-earth L1 libration point orbits. *J Astronaut Sci*. 1994;42(2):207-228.
21. Han D. Orbit transfers for Dawn's Vesta operations: navigation and mission design experience. *23rd Int Symp Sp Flight Dyn*. 2012;(February 2009):1-15. http://trs-new.jpl.nasa.gov/dspace/handle/2014/43029.
22. Davis DC, Khoury F, Howell KC. Phase Control and Eclipse Avoiding in Near Rectilinear Halo Orbits. In: *43rd AAS Guidance, Navigation, and Control Conference*. Breckenridge, CO; 2020.
23. Parrish NL, Bolliger M, Kayser E, et al. Ballistic Lunar Transfers to Near Rectilinear Halo Orbit: Operational Considerations. In: *Space Flight Mechanics Meeting*. Orlando, FL; 2020.
24. Phillips SM, Davis DC, Sweeney DJ. Cloud Computing Methods for Near Rectilinear Halo Orbit Trajectory Design. In: *AAS/AIAA Astrodynamics Specialist Conference*. Portland, ME; 2019.
25. Lee DE. Gateway Destination Orbit Model: A Continuous 15 Year NRHO Reference Trajectory. 2019.
26. Davis DC, Bhatt SA, Howell K, et al. Orbit Maintenance and Navigation of Human Spacecraft at Cislunar Near Rectilinear Halo Orbits. In: *27th AAS/AIAA Space Flight Mechanics Meeting*. San Antonio, TX; 2017.